## Investigation of the Effect of Substrate Morphology on MDCK Cell Mechanical Behavior Using Atomic Force Microscopy

Keyvan Mollaeian, Yi Liu, Siyu Bi, and Juan Ren<sup>a)</sup>
Department of Mechanical Engineering, Iowa State University, Ames, Iowa 50011,
USA

(Dated: 15 June 2019)

Living cells sense and respond to their extracellular environment. Their contact guidance is affected by the underlying substrate morphology. Previous studies of the effect of substrate pattern on the mechanical behavior of living cells were only limited to the quantification of the cellular elasticity. However, how the length and time scales of the cellular mechanical properties are affected by the patterned substrates have yet to be studied. In this study, the effect of the substrate morphology on the biomechanical behavior of living cells was thoroughly investigated using indentation-based atomic force microscopy. The results showed that the cellular biomechanical behavior was affected by the substrate morphology significantly. The elasticity and viscosity of the cells on the patterned PDMS substrates were much lower compared to those cultured on flat PDMS. The poroelastic diffusion coefficient of the cells was higher on the patterned PDMS substrates, specifically on the substrate with 2D pitches. In addition, fluorescence images showed that the substrate topography directly affects the cell cytoskeleton morphology. Together, the results suggested that cell mechanical behavior and morphology can be controlled using substrates with properly designed topography.

Anchorage-dependent cells sense and respond to the underlying substrate<sup>1</sup>. The cells tune their focal adhesions to adapt to their extracellular environment<sup>2</sup>. Recent developments in micro- and nano-scale fabricated materials provide new prospects for the investigation of cell mechanics change affected by substrate  $topographv^{3-6}$ . For instance, it has been reported that patterned substrate affects cell regulation such as migration<sup>7</sup>, gene expression<sup>8</sup>, cell signaling<sup>9</sup>, and cell polarization<sup>10</sup>. However, the effect of the substrate's pattern on cellular mechanical properties at different time and length scales is poorly understood. Thus, to have an in-depth understanding of the substrate effect on cell mechanics, study of the length- and time-dependence of the cell mechanical behavior subject to different substrate patterns is necessary.

Currently, the effect of substrate texture on the cellular behavior has been mostly studied by quantification of the cell Young's modulus at a single measurement depth using atomic force microscopy (AFM) due to its high spatial and nanoscale resolution 11,12. For instance, Mc-Kee et al. (2011) investigated the biomechanical behavior of the HTCEpi cells on patterned substrates using AFM and found that increasing the pitch size of the substrate led to the Young's modulus increase of the cells in the area where the nucleus was present<sup>12</sup>. Rianna et al. (2017) investigated the Hertzian elastic modulus of the cancer cells on PDMSs with nanogroove patterns using AFM and reported that the textures led to a decrease in Young's modulus of the cancer cells compared to the control<sup>13</sup>. However, these methodologies do not account for the biphasic nature of living cells, in which

the porous solid cytoskeletal network is bathed in liquid cytosol<sup>14</sup>. Therefore, poroelastic behavior should be quantified as well to investigate living cell mechanical behavior<sup>15</sup>. Poroelasticity of living cells describes the cells' ability to equilibrate the intracellular pressure when external force stimuli exist, and is represented by the diffusion coefficient, D, which is related to the pore size of the cytoskeleton,  $\xi$ , the elastic modulus, E, and the viscosity of the cytosol,  $\mu^{16}$ . Thus, the quantification of the poroelasticity along with viscoelasticity (i.e., apparent viscosity) and elasticity can provide a complete picture of the cell biomechanics' variation caused by substrate texture. Moreover, since it is well known that the cell mechanical response is length (i.e., indentation depth) dependent<sup>15,17,18</sup> due to heterogeneity of cell structure, it is also necessary to study the cell mechanical behavior under various stimulation depths to understand the effect of substrate's pattern on the length-dependence of cell mechanics.

Polydimethylsiloxane (PDMS) materials have been widely used as common cell culture substrate. Despite the drawbacks of the PDMS such as hydrophobicity, its flexibility, optical transparency, gas permeability, and non-toxicity make it as an appealing substrate for cell studies<sup>19,20</sup>. For instance, PDMS substrates with different rigidities have been used to manipulate the signaling pathway of the neuronal differentiation of the human embryonic stem cells<sup>21</sup>, and it was reported that the primary mouse cortical neurons co-cultured with neurons derived from mouse neural stem cells inside PDMS microconduits generate electrical signal interactions<sup>22</sup>. Therefore, the effect of PDMS substrate topography on mechanical behavior of MDCK cells using AFM force-indentation measurement technique has been investigated in this study. Specifically, mechanical characterization is performed on Madin-Darby canine kidney (MDCK) cells cultured on PDMS substrates of

a) Author to whom correspondence should be addressed. Electronic mail: juanren@iastate.edu.

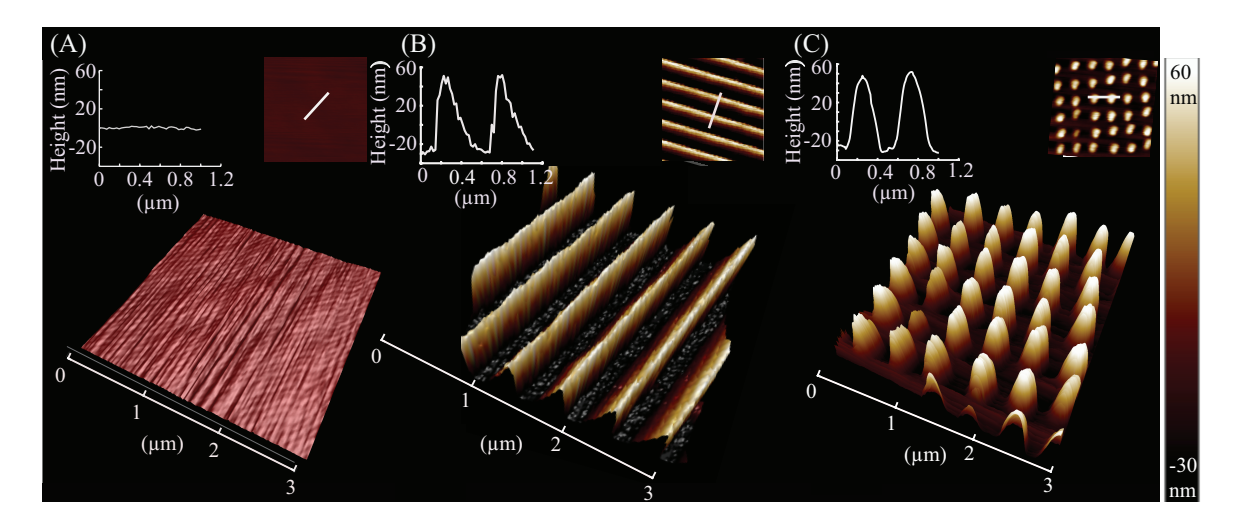


FIG. 1. AFM topography images of (A) flat PDMS, (B) 1D PDMS, and (C) 2D PDMS substrates.

the same base/curing agent ratio with different patterns (flat, ridges (1D) and elevated disks (2D) with 80 nm height and  $0.5 \mu m$  pitch size, see Fig. 1), and the relation between the substrate's texture and cell mechanical behavior (elasticity E, shear modulus G, viscoelasticity  $\eta$ , and poroelasticity D) at different indentation depths is presented. To investigate the effect of substrates' pattern on the biomechanical behavior of the cells, the cells were indented with the indenting velocity of 20  $\mu m/s$  until the desired indentation depths were reached (i.e., the indenting process) and the probe was then rested on the cells for one second (the force-relaxation process). The cell poroelasticity (i.e., D) was quantified through fitting the force-time relaxation curve (i.e., force vs. time response during the force-relaxation process) using the following empirical poroelastic model<sup>14</sup>:

$$\frac{F(t) - F_f}{F_i - F_f} = 0.493e^{-0.822\sqrt{\frac{Dt}{a^2}}} + 0.507e^{-1.348\frac{Dt}{a^2}}.$$
 (1)

where a is the probe-cell contact size during the time force relaxes from  $F_i$  to  $F_f$ . Complete details of AFM mechanical characterization procedure are given in Supplementary Information. Furthermore, the actin filament (F-actin) morphology change caused by different substrate patterns is also investigated. Details on the cell preparation and AFM measurement procedure are presented in the supplementary material.

As shown in Fig. 2, the synthetic structured substrates affect the cellular mechanical behavior significantly. Agreeing with previous studies, the nonlinearity (mechanical property vs. indentation relation) of E, G, and  $\eta$  of the cells seeded on the all PDMS substrates are synchronized with the substrates': all decreased monotonically with the increase of the indentation depth<sup>18,23</sup>. Specifically, the stiffness of the PDMS substrates is decreased by almost 45% when the indentation depth is increased from 300 nm to 500 nm. As a result, E of the cells cultured on the flat, 1D, and 2D PDMS

substrates decreased by 69%, 54%, and 60% when the indentation depth was increased from 325 to 1300 nm, respectively, and similar trend of nonlinearity of G and  $\eta$  were observed for all measured cells on the three substrates as well. This observed similarity in mechanical nonlinearity between cells and substrates is caused by mechanical adaptation of the living cells to the substrate's nonlinear mechanics<sup>18</sup>. However, the diffusion coefficient, D, was monotonically increasing: D increased by 600%, 1050%, and 1700% for the cells seeded on the flat, 1D and 2D PDMS substrates, respectively, when the indentation was quadrupled from 325 nm. This result is consistent with the poroelastic scale law,  $D \sim E\xi^2/\mu$  (where  $\mu$  is the viscosity of the cytosol), that the pore size is more dominant than E in affecting the poroelastic behavior of the cells<sup>14,15</sup>. As the cells are subject to local cytoskeleton stretching at bigger indentations, larger lateral expansion is resulted, which directly leads to larger pore size,  $\xi$ , of the cytoskeleton meshwork. Therefore, the diffusion coefficient increases at higher indentation depth, regardless of the substrate mechanical nonlinearity.

Besides the cell adaptation to substrate mechanical property, the experiment results show that the cell mechanical behavior can be directly altered by the substrate topography. Compared to the values measured from the the control (i.e., cells on the flat PDMS), the Young's modulus of the cells on the 1D PDMS at the indentation depths of 325, 650, 1000, and 1300 nm decreased by 71%, 62%, 67%, and 57%, and the decrease was 67%, 65%, 67%, and 57%, respectively, for the cells cultured on the 2D PDMS. In addition, G and  $\eta$  of the cells on the 1D and 2D PDMSs at each indentation depth reduced by at least 50% and 64%, respectively, with respect to the ones of the control. These reductions are caused by the reduced cell-substrate contact area on the patterned substrates. Previous studies have shown that the smaller contact area on the structured

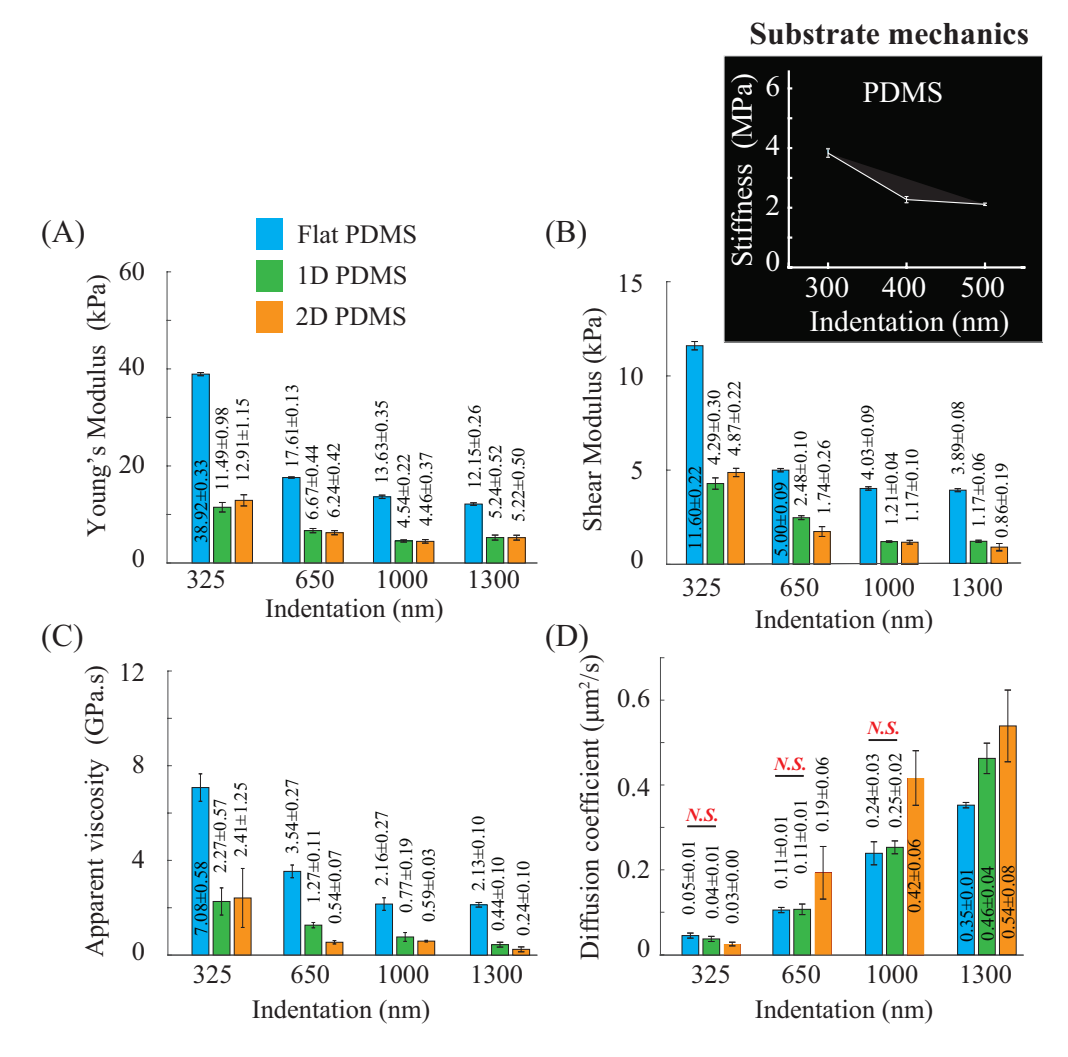


FIG. 2. (A) Young's modulus, (B) shear modulus, (C) apparent viscosity, and (D) diffusion coefficient of MDCK cells seeded on different substrates, respectively, measured at four indentation depths (325, 650, 1000, and 1300 nm) and the indenting velocity of  $20\mu\text{m/s}$ . n=6. Students t-test was performed to analyze the statistical difference: for each indentation, data were compared with respect to the ones measured on the flat PDMS at the same indentation; and for each substrate, the data measured at the minimum indentation (325 nm) for that substrate were chosen as control. A p < 0.05 was yielded for each comparison unless otherwise denoted in the figure (N.S.: not significant.).

substrates (e.g., 1D and 2D PDMS substrates) results in lower focal adhesion and contractility compared to the flat PDMS substrate<sup>24</sup>. Then as a result, lower cellular Young's modulus were observed<sup>24</sup>. Note that the Young's modulus of MDCK cells measured in this study 4-40 kPa is in agreement with previously reported values<sup>25</sup>. Furthermore, the lower contractility of the cells on the structured substrates leads to lower shear stress of the cells<sup>18,26</sup>. Thus, the shear modulus (G=shear stress/shear strain) of the cells seeded on the 1D and 2D PDMSs is lower than that of the control at each indentation depth. Note that E and G values measured for the cells on the 1D and 2D PDMSs are similar indicating that the pattern shape (with the same height and pitch size) does not affect the stiffness of the cells much. Meanwhile, the high degree lateral expansion of the cells seeded on the patterned PDMSs leads to higher

intracellular fluid flow rate (i.e., shear rate). Therefore, the cell apparent viscosity ( $\eta = \text{shear stress/shear}$  rate<sup>27</sup>) measured for the cells on the 1D and 2D PDMSs decreases at each indentation depth compared to that of the cells on the flat PDMS (i.e., control).

However, the diffusion coefficient was higher for the cells on the patterned PDMSs at each indentation depth compared to the values measured on the flat PDMS. Specifically, at the higher indentation depths: with respect to the values measured from the control, D of the cells on the 1D PDMS at the indentation depths of 1000 and 1300 nm increased by 4% and 31%, respectively, and the increase was 75% and 54%, respectively, for the cells seeded on the 2D PDMS. The MDCK cells seeded on the 2D PDMS behave more poroelastic at the measured indentation depths due to the lower contractility and larger expansion of the cells

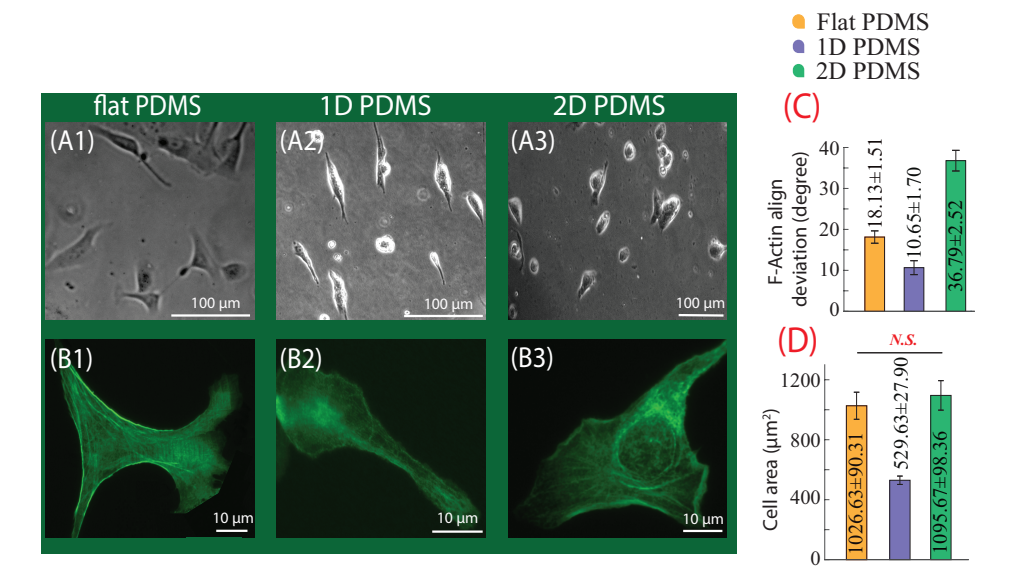


FIG. 3. Example of optical images ((A1)-(A3)) and F-actin cytoskeleton images ((B1)-(B3)) of MDCK cells seeded on the three substrates, respectively. (C) and (D) show the comparison of the F-actin alignment angle deviations and the cell area quantified from the F-actin cytoskeleton on each substrate, respectively. n=10. Students t-test was performed to analyze the statistical difference: data were compared with respect to the ones measured on the flat PDMS. A p < 0.05 was yielded for each comparison unless otherwise denoted in the figure (N.S.: not significant.).

which further result in larger pore size, and thus, bigger diffusion coefficient. It is noticed that the difference of D is not significant at the indentation of 325 nm as the substrate morphology effect is not significant at low measurement depth due to the thick plasma membrane of MDCK cells<sup>28</sup>. Moreover, for the cells seeded on the 1D PDMS, D was not much different compared to that measured on the flat PDMS. We suspect this might be due to the constrained cell morphology on the 1D PDMS. Therefore, we investigated the F-actin cytoskeleton morphology for an in-depth understanding of the biomechanical behavior of the cells.

As can be seen in Fig. 3, the F-actin alignment and the cell shape were guided by the substrate patterns. The alignment angles of F-actin of the cells seeded on the 1D PDMS substrate is more uniform than the other two cases. This is because the F-actin alignment follows the substrate topography patterns <sup>13,24,29</sup>. Specifically, on the 1D substrate, focal adhesions are mostly located on the top surface of the ridges<sup>24,30</sup>, therefore, the cell shape and the F-actin alignment directly follow the direction of the 1D ridges<sup>29,31</sup>. Thus, the cells are stretched along one direction, i.e., the cells are thin and long, and the cell area is smaller compared to the other two cases. Similarly, the cells on the 2D PDMS are stretched along multiple directions (i.e., with square or round shapes) due to the pitches on the substrate. As a result, the larger F-actin alignment deviation and cell area are yielded<sup>24,32,33</sup>. Different from the patterned substrates, the flat PDMS allows the cell membrane and cytoskeleton to expand freely, i.e., the cell shape is more random. Thus, the F-actin alignment

deviation is between the values for the other two cases, and the cell area is relatively large. As a result, the difference in F-actin cytoskeleton morphology directly reflected the cell mechanical behavior difference during the biomechanical measurement since the cytoskeleton morphology has been shown to play a fundamental role in cellular mechanics<sup>18</sup>.

The cell morphology images and the quantified F-actin cytoskeleton data together with the cell biomechanical characterization results indicate that the substrate topography affects the cell biomechanical behavior and the cell morphology, simultaneously. Therefore, the results of this study suggest that it is possible to achieve cell mechanical behavior and morphology control using substrates with properly designed topography patterns. For further studies, it would be interesting to investigate the effect of substrate topography on cytoskeleton morphology in details, and quantify the relation between the cytoskeleton morphology and cell mechanical properties to provide more information on cell mechanical behavior control through extracellular environment.

See supplementary material for the details of materials, PDMS and cell preparation, and AFM mechanical characterization procedure.

This work was supported by the National Science Foundation (NSF) [CMMI-1634592], [CMMI-1751503], and Iowa State University. We also thank Dr. Meng Lu from Iowa State University for generously providing the PDMS substrates.

- <sup>1</sup>D. E. Discher, P. Janmey, and Y.-l. Wang, Science **310**, 1139 (2005).
- <sup>2</sup>Y. Abidine, A. Constantinescu, V. M. Laurent, V. S. Rajan, R. Michel, V. Laplaud, A. Duperray, and C. Verdier, Biophysical journal 114, 1165 (2018).
- <sup>3</sup>B. Liu, H. Monshat, Z. Gu, M. Lu, and X. Zhao, Analyst **143**, 2448 (2018).
- <sup>4</sup>S. Shabaniverki, S. Thorud, and J. J. Juárez, MethodsX **5**, 1156 (2018).
- <sup>5</sup>S. Shabaniverki, S. Thorud, and J. J. Juarez, Chemical Engineering Science 192, 1209 (2018).
- <sup>6</sup>P. S. Yadav, S. Gulec, A. Jena, S. Tang, S. Yadav, D. Katoshevski, and R. Tadmor, Surface Topography: Metrology and Properties 6, 045007 (2018).
- <sup>7</sup>X. Jiang, D. A. Bruzewicz, A. P. Wong, M. Piel, and G. M. Whitesides, Proceedings of the National Academy of Sciences 102, 975 (2005).
- <sup>8</sup>S. A. Park, I. A. Kim, Y. J. Lee, J. W. Shin, C.-R. Kim, J. K. Kim, Y.-I. Yang, and J.-W. Shin, Journal of bioscience and bioengineering 102, 402 (2006).
- <sup>9</sup>G. Giannone and M. P. Sheetz, Trends in cell biology **16**, 213 (2006).
- <sup>10</sup>E. W. Chan and M. N. Yousaf, Molecular BioSystems 4, 746 (2008).
- $^{11}\dot{\mathrm{S}}.$  Xie and J. Ren, Mechatronics 57, 86 (2019).
- <sup>12</sup>C. T. McKee, V. K. Raghunathan, P. Russell, and C. J. Murphy, Microscopy and Analysis-UK, 25 (2011).
- <sup>13</sup>C. Rianna, P. Kumar, and M. Radmacher, in Seminars in cell & developmental biology, Vol. 73 (Elsevier, 2018) pp. 107–114.
- <sup>14</sup>E. Moeendarbary, L. Valon, M. Fritzsche, A. R. Harris, D. A. Moulding, A. J. Thrasher, E. Stride, L. Mahadevan, and G. T. Charras, Nature materials 12, 253 (2013).
- <sup>15</sup>K. Mollaeian, Y. Liu, S. Bi, and J. Ren, Journal of the mechanical behavior of biomedical materials 78, 65 (2018).
- <sup>16</sup>G. T. Charras, T. J. Mitchison, and L. Mahadevan, Journal of cell science **122**, 3233 (2009).

- <sup>17</sup>Y. Liu, K. Mollaeian, and J. Ren, Micron **116**, 108 (2019).
- <sup>18</sup>K. Mollaeian, Y. Liu, S. Bi, Y. Wang, J. Ren, and M. Lu, International journal of molecular sciences 19, 3461 (2018).
- <sup>19</sup>S. Halldorsson, E. Lucumi, R. Gómez-Sjöberg, and R. M. Fleming, Biosensors and Bioelectronics 63, 218 (2015).
- <sup>20</sup>J. N. Lee, X. Jiang, D. Ryan, and G. M. Whitesides, Langmuir 20, 11684 (2004).
- <sup>21</sup>S. Willerth, in *Engineering Neural Tissue from Stem Cells* (Elsevier, 2017) pp. 127–158.
- <sup>22</sup>Y. Takayama, H. Moriguchi, K. Kotani, T. Suzuki, K. Mabuchi, and Y. Jimbo, Biosystems 107, 1 (2012).
- <sup>23</sup>M. Gupta, B. R. Sarangi, J. Deschamps, Y. Nematbakhsh, A. Callan-Jones, F. Margadant, R.-M. Mège, C. T. Lim, R. Voituriez, and B. Ladoux, Nature communications 6, 7525 (2015).
- <sup>24</sup>A. I. Teixeira, G. A. Abrams, P. J. Bertics, C. J. Murphy, and P. F. Nealey, Journal of cell science 116, 1881 (2003).
- <sup>25</sup>F. Sorba, A. Poulin, R. Ischer, H. Shea, and C. Martin-Olmos, Lab on a Chip (2019).
- <sup>26</sup>A. J. Engler, M. A. Griffin, S. Sen, C. G. Bönnemann, H. L. Sweeney, and D. E. Discher, J Cell Biol 166, 877 (2004).
- <sup>27</sup>R. E. Wells and E. W. Merrill, Science **133**, 763 (1961).
- <sup>28</sup>B. Sorce, C. Escobedo, Y. Toyoda, M. P. Stewart, C. J. Cattin, R. Newton, I. Banerjee, A. Stettler, B. Roska, S. Eaton, et al., Nature communications 6, 8872 (2015).
- <sup>29</sup>R. Flemming, C. J. Murphy, G. Abrams, S. Goodman, and P. Nealey, Biomaterials **20**, 573 (1999).
- <sup>30</sup>K. Matsuzaka, F. Walboomers, A. De Ruijter, and J. A. Jansen, Clinical oral implants research 11, 325 (2000).
- <sup>31</sup>P. T. Ohara and R. C. Buck, Experimental cell research 121, 235 (1979).
- $^{32}\mbox{H}.$  Sunami, I. Yokota, and Y. Igarashi, Biomaterials science 2, 399 (2014).
- <sup>33</sup>T. Yeung, P. C. Georges, L. A. Flanagan, B. Marg, M. Ortiz, M. Funaki, N. Zahir, W. Ming, V. Weaver, and P. A. Janmey, Cell motility and the cytoskeleton 60, 24 (2005).